Biogeosciences Discuss., 9, 5445–5469, 2012
www.biogeosciences-discuss.net/9/5445/2012/
doi:10.5194/bgd-9-5445-2012

Biogeosciences Discussions

The role of alkalinity generation in controlling the fluxes of CO_2 during exposure and inundation on tidal flats

P. A. Faber[1], A. J. Kessler[1], J. K. Bull[1], I. D. McKelvie[2,3], F. J. R. Meysman[4], and P. L. M. Cook[1]

[1]School of Chemistry, Monash University, Victoria 3800, Australia
[2]School of Chemistry, The University of Melbourne, Victoria 3010, Australia
[3]School of Geography, Earth and Environmental Sciences, University of Plymouth, Plymouth PL48AA, UK
[4]Department of Ecosystem Studies, Royal Netherlands Institute for Sea Research (NIOZ), Korringaweg 7, 4401 NT Yerseke, The Netherlands

Received: 2 April 2012 – Accepted: 22 April 2012 – Published: 9 May 2012

Correspondence to: P. A. Faber (peter.faber@monash.edu)

Published by Copernicus Publications on behalf of the European Geosciences Union.

Abstract

Dissolved inorganic carbon, CO_2 and alkalinity fluxes from intertidal sediments were investigated during periods of exposure and inundation, using laboratory core incubations, field data and reactive transport model simulations. In the incubations and field data, it was found that during periods of alkalinity production, the flux of dissolved inorganic carbon (DIC) out of the sediment was significantly greater during inundation periods. This alkalinity production was attributed to the accumulation of reduced sulfur species within the sediment. This finding was supported by computational simulations which indicated that large amounts of sulfate reduction and reduced solute burial (FeS) induce an alkalinity flux from the sediment during high tide conditions. As the fate of sulfide is controlled by Fe, the sensitivity of alkalinity flux to Fe concentrations was investigated, and it was found that amount of reactive Fe in the sediment was a major driver of net alkalinity production. The finding the CO_2 fluxes can be significantly lower than total metabolism during exposure has implications for how total metabolism is quantified on tidal flats.

1 Introduction

Tidal flats are highly dynamic and biogeochemically active environments, that are characterised by the deposition of allochthonous organic matter as well as high in-situ rates of primary production by microphytobenthos (Joye et al., 2009). The quantification of organic carbon production and mineralisation in these environments is complicated by the fact that tidal flats are periodically inundated. This means that fluxes of inorganic carbon should ideally be measured both during inundation (as dissolved inorganic carbon DIC = $[CO_2] + [HCO_3] + [CO_3]$) and exposure (as gaseous CO_2). In practice, the quantification of inorganic carbon fluxes during the inundation of tidal flats is logistically complex because they are covered by a shallow layer of turbid water, and often experience high currents. Moreover, the determination of DIC in aqueous samples is

BGD
9, 5445–5469, 2012

also more time consuming and technically challenging than the analysis of CO_2 in gas samples. As a consequence, most studies of metabolism on tidal flats only measure gaseous fluxes of CO_2 during exposure (Migné et al., 2005; Middelburg et al., 1996).

Relatively few studies have included direct measurement of inorganic carbon fluxes during both exposure and inundation of tidal flats, and moreover, these studies show different outcomes. Alongi et al. (1999) found very similar exchange rates during both inundation and exposure. By contrast, Gribsholt and Kristensen (2003) and Cook et al. (2004) found consistently higher rates of inorganic carbon exchange during inundation on un-vegetated tidal flat sediments, where the flux during inundation increased by a factor of ~ 2. A number of possible explanations exist for these differences. Firstly, solute transport processes are very different between inundation and exposure periods. During inundation, all three forms of the carbonate system (CO_2, HCO_3^- and CO_3^{2-}) can be transported across the sediment interface, whereas during exposure, only CO_2 can diffuse into the atmosphere. Furthermore, bio-irrigation is well known to enhance solute exchange in sediments (Kristensen, 1988). This process will cease upon emersion, and would result in a reduction of the CO_2 flux during exposure as compared to the inundated DIC flux. Secondly, alkalinity generation, caused by the burial of reduced metal sulfides and/or calcium carbonate dissolution, is often observed at high rates in shallow waters and intertidal sediments (Thomas et al., 2009; Cook et al., 2004; Ferguson et al., 2003b). Alkalinity cannot escape the sediment during low tide, and so will tend to accumulate near the sediment-water interface. This will lead to a shift towards increased HCO_3^- and CO_3^{2-} and decreased CO_2, and hence, a reduced gaseous CO_2 flux during exposure.

However, there are also reasons why the CO_2 flux might be enhanced during exposure. A change in CO_2 transfer during exposure to the atmosphere may occur due to the higher diffusion of CO_2 in the atmosphere (10^{-5} compared to $10^{-9}\,m^2\,s^{-1}$) and the decreased thickness of the diffusive boundary layer during exposure (Brotas et al., 1990).

BGD
9, 5445–5469, 2012

To date, none of these factors have been explored, experimentally or theoretically. A basic understanding of the exchange dynamics of inorganic carbon is required for the design of studies aiming to quantify the fluxes of inorganic carbon between tidal flats and the atmosphere and coastal waters. Here, we used data from controlled laboratory experiments, and a numeric diagenetic model to investigate the dynamics of inorganic carbon exchange in the intertidal zone. In particular, we focus on the role of alkalinity generation by anaerobic respiration in the retardation of the CO_2 efflux during exposure relative to DIC export to the water column.

2 Materials and methods

2.1 Experimental

Muddy sediment (Grain size: 48 % 300 µm–1 mm; 8 % 200–300 µm; 39 % 100–200 µm; 5 % 62–100 µm and porosity = 0.81 ml water cm^{-3}) sediment was collected from an intertidal flat located in the Yarra Estuary, Australia (37.833° S, 145.0229° E). The sediment was sieved (1 mm mesh) to remove macrofauna and homogenised. The total inorganic carbon content of the sediment was < 0.1 % w/w. The sediment was then placed in a shallow tray and gently stirred whilst being aerated for 1 day to oxidise reduced solutes before being packed into 8 core liners (7 cm diameter) to a depth of 5 cm. The cores had stirrer bars inserted to gently stir the water column. A peristaltic pump system transferred ambient sea water collected from Port Phillip Bay in and out of the cores (salinity = 35, temperature = 20 °C). The pumping regime followed a regular six hourly cycle that mimicked a semi-diurnal tide. The inlet of the tubes in the core was recessed slightly into the sediment surface, so that all the overlying water could be removed, leaving no ponding of water on the surface during emersion. Carbon mineralisation processes in natural systems can be highly dynamic reflecting pulsed inputs of organic matter (OM), for example, deposition of phytodetritus. This pulsed occurrence of carbon mineralisation is highly relevant, driving cycles of solute reduction and oxidation,

BGD
9, 5445–5469, 2012

which in turn drives alkalinity production and consumption. To simulate a pulse of organic matter, half of the cores had 0.38 g baker's yeast added to them after 71 days (+OM treatment), while the remaining cores did not receive this organic matter input (−OM). During inundation, the flux of DIC was determined by covering the cores with sealed lids and taking 4–5 water samples during sediment inundation. The DIC flux was determined as the slope of DIC concentration versus time multiplied by the water height. The pH was simultaneously measured as the water sample for alkalinity was taken. During exposure, the flux of gaseous CO_2 was measured by sampling the gas headspace of the sealed core. Again, the CO_2 flux was determined as the slope of CO_2 concentration versus time multiplied by the headspace height. CO_2 was sampled using evacuated 3 ml draw blood collection vials (Vacutainers, Becton Dickinson) and analysed using Flow Injection Analysis (Satienperakul et al., 2004). Alkalinity samples were filtered (Bonnet, 0.45 µm polyethersulfone) and preserved with 20 µl $HgCl_2$ (6 % w/v) and the concentration was determined using a modified Gran titration (Almgren et al., 1983). pH was determined using a pH electrode (Hach PHC301 connected to an HQ40d meter), calibrated with NBS buffers. DIC concentrations in the water column were calculated using alkalinity and pH, with the constants found in Roy et al. (1993). The method for total Fe analysis of the dried sediment was modified from Lord (1982), using a 24 h citrate/bicarbonate/dithionite extraction for easily extractable Fe, followed by a 24 h concentrated nitric acid digestion. The extracts were then analysed using atomic absorption spectroscopy (AAS).

2.2 Model formulation

The reactive transport model follows the standard formulation for early diagenetic models of marine sediments (Boudreau, 1997; Meysman et al., 2003). The model simulates the depth profiles of solutes and solids, as well as the fluxes across the sediment-water

BGD
9, 5445–5469, 2012

interface, based on the mass balance equations

$$\text{Solutes: } \varphi \frac{\partial C_i^{\mathrm{PW}}}{\partial t} = \frac{\partial}{\partial x}\left[\varphi D_i \frac{\partial C_i^{\mathrm{PW}}}{\partial x}\right] + \sum_k \nu_{i,k} R_k$$

$$\text{Solids: } (1-\varphi) \frac{\partial C_i^{S}}{\partial t} = \frac{\partial}{\partial x}\left[(1-\varphi) D_{\mathrm{B}} \frac{\partial C_i^{S}}{\partial x}\right] + \sum_k \nu_{i,k} R_k$$

where C_i^{PW} and C_i^{S} are the concentrations of a solute and solid compound, respectively. No advective processes are included in the model, as negligible sedimentation during the incubations was assumed. The porosity φ is assumed constant with depth. For solutes, the only transport process is molecular diffusion. The diffusion coefficient D_i is calculated as a function of temperature and salinity using the R package marelac (Soetaert, 2010) and subsequently corrected for tortuosity according to the modified Wiessberg relation of Boudreau (1996). For solids, the dominant transport processes is bioturbation, which is modelled as a diffusive process (Meysman et al., 2010). The biodiffusion coefficient D_{B} is assumed to be constant with depth. The quantities R_k represent the reaction rates, where $\nu_{i,k}$ is the stoichiomeric coefficient of the i-th species in the k-th reaction. The reaction set includes three mineralisation pathways (aerobic respiration, dissimilatory iron reduction and sulfate reduction) for two fractions of organic matter (fast and slow decaying), the formation of iron sulfide and pyrite, and the reoxidation of reduced compounds in pore water (ferrous iron, free sulfide) and solid phase (iron sulfides and pyrite). The full set of 13 reactions is given in Table 1. The rate expressions for these reactions follow the standard kinetic rate laws and are given in Table 2.

BGD
9, 5445–5469, 2012

2.3 Boundary conditions and initial state

The cyclic process of inundation and exposure was simulated by regular switching between two sets of boundary conditions. Under inundation, the concentration of solutes at the sediment-water interface was fixed to that of the overlying water, while a fixed flux was imposed for the solids. These fluxes were set to zero for all solid components during the whole simulation period (zero deposition assumed – see above), apart from organic matter, which received a pulse input at 71 days. To model this pulse input, the organic matter was added uniformly to the top 2 mm of the sediment at a total concentration of $\sim 2500\,\mu mol\ CH_2O\,g^{-1}$ dry sediment and fractionated between the fast-decaying fraction (75 %) and the slow-decaying fraction (25 %).

Under exposed conditions, only the volatile solutes O_2 and CO_2 have an exchange with the overlying atmosphere, which is modelled using the convective boundary flux $J = k_d\left(C^{eq} - C\right)$ with k_d the piston velocity and C^{eq} the gas concentration in equilibrium with the atmosphere. At the lower boundary of the sediment domain a no-flux condition was imposed for all compounds over the whole simulation period.

Reduced Fe (FeS and FeS_2) concentration was initially set to 0 and the O_2 concentration in the pore water was set to equilibrium with atmospheric concentration. A uniform profile of slow-decaying organic matter ($\sim 2500\,\mu mol\ CH_2O\,g^{-1}$ dry sediment), and either 19 or 95 $\mu mol\ Fe\,g^{-1}$ dry sediment was imposed. These latter values were determined to be extreme low and high Fe concentrations, as measured by a total Fe extraction at the conclusion of the experiment.

2.4 Numerical model solution

A numerical solution procedure was implemented in the open-source programming language R as fully detailed in Soetaert and Meysman (2012). A reactive transport model essentially consists of one partial differential equation (PDE) for each compound. Following the method-of-lines, the R-package ReacTran uses a finite difference scheme to expand the spatial derivatives of the PDEs over the sediment grid. This grid was

BGD
9, 5445–5469, 2012

obtained by dividing the sediment domain (thickness L = 5 cm, the approximate depth of the sediment cores in the incubation experiment) into a uniform grid of 100 sediment layers. After finite differencing, the resulting set of ODEs was integrated using the stiff equation solver vode from the R-package deSolve.

2.5 Description of model runs

The model was set up to simulate the tidal cycles imposed in the laboratory core incubation experiments, which were exposed and inundated alternately every 6 h.

The model simulations provide flux estimates at each point in time. The fluxes of TA and DIC during inundation and CO_2 fluxes during exposure are reported as the mean over the 6-h exposure/inundation period. The simulation extended over 120 days (i.e. 240 tidal cycles), with a pulse of organic matter added on day 70, simulating the addition of the organic matter source in the laboratory experiments. Table 3 lists an overview of parameters values used in model simulations. These were determined from measured properties, literature values or calibrated to the available dataset. All parameter values were kept constant during the whole simulation period (apart from the organic matter input).

2.6 Sensitivity model runs

The sensitivity of CO_2 flux to the piston velocity was investigated using simulations, where the piston velocity was varied from 0.05 to 5 cm h^{-1}. In each simulation, the initial FeOOH concentration was 19 µmol Fe g^{-1} dry sediment. For each value of the piston velocity, the average flux of CO_2 during exposure was calculated over the complete simulation period (30 tidal cycles). This procedure was repeated for three different initial values of organic matter concentration (2500, 1000 and 600 µmol C g^{-1} dry sediment for the slow-decaying fraction, and 5, 2.5 and 1.3 µmol C g^{-1} dry sediment for the fast-decaying fraction, respectively), to investigate the sensitivity of CO_2 flux to the piston velocity under different amounts of organic matter loading.

BGD
9, 5445–5469, 2012

The availability of reactive oxidised iron (FeOOH) controls alkalinity production in the sediment, and hence, we performed a second series of simulations to investigate the sensitivity of the model towards the initial sedimentary FeOOH concentration. To determine the effect of FeOOH availability on TA production, simulations were run with a fixed initial concentration of CH_2O ($\sim 2500\,\mu mol\ CH_2O\ g^{-1}$ dry sediment) but with various FeOOH concentrations (7.6, 19 and 95 $\mu mol\ Fe\ g^{-1}$ dry sediment). The values of 19 and 95 $\mu mol\ Fe\ g^{-1}$ dry sediment are the low and high estimates of sediment FeOOH concentrations in the core experiment sediment, respectively. The value of 7.6 $\mu mol\ Fe\ g^{-1}$ dry sediment was chosen as a low value for a comparison with our estimates.

3 Results

3.1 Experimental

There was little variation in the DIC fluxes over the entire course of the experiment in the –OM treatment with a mean value of 1.3 $mmol\ m^{-2}\ h^{-1}$ over the 120 days (Fig. 1). In the +OM treatment, DIC fluxes were the same as the –OM treatment within experimental uncertainty in the first 70 days of the experiment before the organic matter was added (Fig. 1). After the organic matter addition, DIC fluxes substantially increased to a maximum of $\sim 5.0\,mmol\ m^{-2}\ h^{-1}$, and then decreased again to $\sim 2.0\,mmol\ m^{-2}\ h^{-1}$ over a time period of 40 days after organic matter addition. Alkalinity fluxes were initially high in both –OM and +OM treatments, steadily decreasing from $> 1.4\,mmol\ m^{-2}\ h^{-1}$ at the start of the experiment to attain a negligible alkalinity flux after 60 days. The most likely explanation for this observation is that there was an initial formation of a large pool of iron sulfides. Initially, a large pool of Fe(III) is formed during sediment pretreatment, which is subsequently gradually depleted and turned into metal sulfides. Dissimilatory iron reduction produces alkalinity (TA : DIC = 8, see R9 in Table 2), and so alkalinity production will decrease over time. After the pulsed addition of organic

BGD
9, 5445–5469, 2012

matter, alkalinity fluxes increased rapidly to a maximum of 3.0 mmol m^{-2} h^{-1} before decreasing again rapidly. The CO_2 fluxes during exposure were initially very low in both treatments (~ 0.10 mmol m^{-2} h^{-1}). In the −OM treatment, the CO_2 flux increased after 60 d, coinciding with the decrease and cessation of alkalinity fluxes (fluxes not significantly different from zero, shown by the error bars). In the +OM treatment, there was an increase in CO_2 fluxes after the addition of organic matter, reaching a maximum of ~ 2.5 mmol m^{-2} h^{-1}. The CO_2 fluxes decreased again to ~ 0.60 mmol m^{-2} h^{-1} at the conclusion of the experiment.

3.2 Model simulations

To match with the laboratory experiments, the data from the model were truncated before 20 days (Fig. 1). From day 20 to 70, the simulation yielded inundated DIC fluxes between ~ 1.2 and ~ 1.4 mmol m^{-2} h^{-1}. Immediately after the OM addition at day 70, the DIC flux increased to a maximum of ~ 5.7 mmol m^{-2} h^{-1}. The TA flux decreased from ~ 0.48 to ~ 0.40 mmol m^{-2} h^{-1} before the OM addition, then increased to a maximum of ~ 0.74 mmol m^{-2} h^{-1} after the addition. The CO_2 flux during exposure was between ~ 0.66 and ~ 1.0 mmol m^{-2} h^{-1} before the OM addition, and rose to a maximum of ~ 3.6 mmol m^{-2} h^{-1} after the addition of the OM, then decreasing again to ~ 1.2 mmol m^{-2} h^{-1} by the end of the simulation. The peak flux during the simulation is shifted relative to the core incubations, due to a delay in the organic matter mineralisation. This is expected, as the bacterial community first needs to grow to consume the bioavailable organic matter. In the computer simulation, no lag phase occurs, as the model formulation does not include population growth, and thus assumes an instantaneous response of microbial metabolism.

In the model simulations, DIC fluxes were consistently higher during inundation than CO_2 fluxes during the corresponding exposure periods (Fig. 2). The discrepancy between DIC and CO_2 fluxes appears to increase with increasing respiration, shown by the divergence of the simulation data from the 1 : 1 line as DIC flux increases. This

BGD
9, 5445–5469, 2012

pattern was very similar to that previously observed for intact sediments collected from tidal flats (Cook et al., 2004) (Fig. 2).

The fluxes of CO_2 during exposure and DIC and TA during emersion were highly sensitive to initial Fe concentrations in the sediment. This can be evaluated by calculating the mean fluxes over the period before organic matter pulse (Fig. 3). The high Fe concentration resulted in a lower CO_2 flux during exposure (~ 0.65 vs. $\sim 0.35\,\mathrm{mmol\,m^{-2}\,h^{-1}}$ for the 19 and $95\,\mu\mathrm{mol\,Fe\,g^{-1}}$ dry sediment). There was also a large discrepancy between alkalinity fluxes, where the high Fe concentration resulted in a higher TA flux ($0.80\,\mathrm{mmol\,m^{-2}\,h^{-1}}$ versus $1.4\,\mathrm{mmol\,m^{-2}\,h^{-1}}$ for the 19 and $95\,\mu\mathrm{mol\,Fe\,g^{-1}}$ dry sediment simulations). The difference between DIC fluxes were smaller, with a flux of $\sim 1.8\,\mathrm{mmol\,m^{-2}\,h^{-1}}$ for the simulation with $95\,\mu\mathrm{mol\,Fe\,g^{-1}}$ dry sediment, and $\sim 1.6\,\mathrm{mmol\,m^{-2}\,h^{-1}}$ for the simulation with $19\,\mu\mathrm{mol\,Fe\,g^{-1}}$ dry sediment.

4 Discussion

4.1 Alkalinity producing reactions

The production of alkalinity can be attributed to several key processes; ammonia release, net denitrification, net sulfate reduction and to a lesser extent, dissolved organic carbon (Hammond et al., 1999). Berner et al. (1970) proposed the idea of sulfate reduction as an alkalinity producing process. It was noted that sulfate reduction coupled with the precipitation of the stable iron sulfides FeS and FeS_2 produces one mole of alkalinity per mole of carbon mineralised (Berner et al., 1970):

$$6CH_2O + 3SO_4^{2-} + 2FeOOH \rightarrow FeS + FeS_2 + 6HCO_3^- + 4H_2O$$

In this representation of sulfate reduction, iron is significant only as a controller of reduced sulfur burial, thus indirectly controlling net alkalinity production by preventing sulfide reoxidation.

BGD
9, 5445–5469, 2012

Hu and Cai (2011) reviewed the factors controlling alkalinity generation in ocean margins in sediment and concluded that the burial of pyrite and the denitrification of NO_3^- derived from the continents were the only net sources of alkalinity in ocean margin sediments. As the cycling of sulfur is closely linked with iron, we included both sulfur and iron geochemistry in the diagenetic model. In our experiments, denitrification was unlikely to be a significant source of alkalinity generation because of the lack of NO_3^- in the overlying water used in our incubations. Consequently, we did not model the effect of denitrification on alkalinity in this model. We are confident that the model used here represents the critical anaerobic alkalinity-generating processes that are important in our experimental set up.

4.2 Agreement of simulations with experimental data

There was a general agreement between experimental data and the model predictions, which showed that DIC fluxes from the sediment during tidal inundation are higher than CO_2 fluxes during exposure. This difference was most pronounced at the start of the experiment and after the addition of organic matter. At the start of the experiments there was a rapid alkalinity generation which can be explained by the formation of FeS as the Fe(III) initially present within the surface sediment was reduced and buried. After the pulse of organic matter, the oxygen concentration in the sediment is reduced, and a higher rate of anaerobic carbon mineralisation takes place, once again leading to increased rates of reduced sulfur production, FeS burial and alkalinity production. In our simulations, reduced sulfur production continues after FeOOH is exhausted, but it is reoxidised as it diffuses into the oxygenated surface layers of sediment. Nonetheless, an alkalinity flux is produced, as there is some storage of H_2S in the sediment. This flux eventually became negative in simulations performed with low amounts of organic matter, as sulfide reoxidation became faster than sulfide production (data not shown).

The dynamics of this simulation/experiment have strong environmental relevance being representative of a resuspension event or the deposition of fresh sediment from the catchment and the deposition of organic matter. This highlights the importance

BGD
9, 5445–5469, 2012

of environmental dynamics in controlling the relative loss of CO_2 and DIC from intertidal sediment. Indeed, in coastal sediments, periodically high fluxes of alkalinity are observed following periods of high organic matter input (Ferguson et al., 2003a). Hargrave and Phillips (1981) describe the significance of short term organic matter deposition, with high supply rates, relative to mineralisation rates, causing a burial of organic matter in deeper, anoxic layers of the sediment.

4.3 Model sensitivity towards piston velocity

There was a linear relation between initial organic matter content (or total mineralisation) and asymptotic CO_2 efflux, at piston velocities $> 1\,cm\,h^{-1}$ (Fig. 4). Decreasing the piston velocity below $0.5\,cm\,h^{-1}$ reduced CO_2 fluxes during sediment exposure. This can be attributed to the slower release of CO_2 for a given CO_2 concentration gradient, and a slower flux of O_2 into the sediment resulting in less aerobic respiration. Indeed, we found the rate of aerobic respiration to decrease with decreasing piston velocity (data not shown). In the first instance, it is expected that the alkalinity flux would remain constant upon changing piston velocity. It was noted, however, that there was an increase in alkalinity production as the piston velocity was decreased indicating that anaerobic respiration accounted for a greater proportion of the total respiration, and oxygen penetration was decreased. Higher respiration rates were more sensitive to decreasing piston velocities due to a faster rate of CO_2 production, and O_2 consumption. For the remainder of the simulations, the piston velocity was fixed at $1\,cm\,h^{-1}$, the lowest of values found by various researchers across the water-air interface in estuarine and riverine systems, as summarised by Raymond et al. (2000). Our simulations showed a piston velocity above this value did not affect CO_2 fluxes (Fig. 3).

BGD
9, 5445–5469, 2012

4.4 Model sensitivity towards sedimentary iron

The sensitivity of the model to Fe suggests that the delivery of fresh (oxidised) Fe controls how much mineralised carbon is exported to the atmosphere versus alkalinity. In the simulation, a large amount of Fe leads to a higher rate of alkalinity production through FeS_2 burial, and a corresponding lower rate of CO_2 production (Fig. 3). The sensitivity of the model to Fe agrees with the literature (Hu and Cai, 2011; Berner et al., 1970), which points out that FeS_2 burial is the most important process controlling alkalinity production. The present work shows that in high carbon systems such as intertidal sediments, Fe will be the limiting species in pyrite burial, despite the role of carbon as the mediating species in pyrite burial globally (Hu and Cai, 2011).

The temporal change of TA fluxes produced in the profile also differs considerably, as TA flux stabilises after 30 days in the simulations with the lower Fe concentrations, whereas at higher Fe concentrations, TA flux continues to increase. This is due to the reduction of all the oxidised Fe, creating a lower net production of alkalinity. For simulations with little or no Fe, there is a temporary sink of HS^- in the sediment during intense alkalinity production. Subsequent alkalinity consumption occurs as the HS^- is re-oxidised. During periods where respiration is extremely high, HS^- has the potential to by-pass the small oxic zone in the sediment, and so the HS^- can reach the water column before it is re-oxidised. In this situation, the numeric simulation will show a net alkalinity flux from the sediment. In reality, immediate re-oxidation of HS^- in the overlying water column will directly consume this alkalinity.

With regard to carbon budgets, the effect of anaerobic carbon metabolism is important as higher alkalinity export to the ocean creates a higher CO_2 buffering capacity for the uptake of atmospheric CO_2. The effect of anaerobic alkalinity production on atmospheric carbon uptake in coastal seas has been estimated at up to 60 % of the total uptake (Thomas et al., 2009). This is an upper estimate, as it neglects alkalinity consumed during nitrification. Increased organic carbon loadings in estuaries has been linked with anthropogenic land use (Abril et al., 2002) contributing an anthropogenic

BGD
9, 5445–5469, 2012

carbon source to the atmosphere. In regions with high anthropogenic disturbance, large amounts of terrestrial carbon is exported towards coastal oceans (Frankignoulle et al., 1996, 1998). Much of this is aerobically degraded, as shown by extremely high pCO_2 values, but a portion of this may be exported as alkalinity, partially negating an anthropogenic carbon source to the atmosphere. Indeed, more anthropogenically disturbed catchments will also export more sediment and hence more Fe(III) (Asselman et al., 2003; Walling, 1999) to estuaries, which will partially offset larger CO_2 emissions from increased labile organic carbon export to estuaries.

5 Conclusions

The laboratory data and field data (Cook et al., 2004) and computer simulations clearly show that CO_2 fluxes during exposure on tidal flats are likely to under-estimate total carbon mineralisation. This finding has clear implications for research in this field, given that total inorganic carbon fluxes for intertidal sediments have generally been estimated using only gaseous CO_2 fluxes on the exposed sediments (Migné et al., 2005; Middelburg et al., 1996). The results of this study demonstrate the importance of considering both exposed and inundated fluxes in studies of intertidal metabolism, which may be quite different, depending on the extent to which there is a net accumulation of reduced solutes.

Acknowledgement. P. Faber acknowledges the assistance of an Australian Postgraduate Association scholarship. This work was supported by a Monash University faculty of science early career researcher grant, as well as Monash researcher accelerator grant to PC. We thank Hans Røy for stimulating discussions on this work.

BGD
9, 5445–5469, 2012

References

Abril, G., Nogueira, M., Etcheber, H., Cabecadas, G., Lemaire, E., and Brogueira, M.: Behaviour of organic carbon in nine contrasting European estuaries, Estuar. Coast. Shelf Sci., 54, 241–262, 2002.

Almgren, T., Dyrssen, D., and Fonselius, S.: Determination of alkalinity and total carbonate., in: Methods of Seawater Analysis, edited by: Grasshoff, K., Ehrhardt, M., and Kremling, K., Springer-Verlag, Chemie, Weinheim, 99–123, 1983.

Alongi, D., Tirendi, F., Dixon, P., Trott, L., and Brunskill, G.: Mineralization of organic matter in intertidal sediments of a tropical semi-enclosed delta, Estuar. Coast. Shelf Sci., 48, 451–467, 1999.

Asselman, N. E. M., Middelkoop, H., and Van Dijk, P. M.: The impact of changes in climate and land use on soil erosion, transport and deposition of suspended sediment in the River Rhine, Hydrol. Process., 17, 3225–3244, 2003.

Berner, R. A., Scott, M. R., and Thomlinson, C.: Carbonate alkalinity in the pore waters of anoxic marine sediments, Limnol. Oceanogr., 544–549, 1970.

Boudreau, B. P.: The diffusive tortuosity of fine-grained unlithified sediments, Geochim. Cosmochim. Acta, 60, 3139–3142, 1996.

Boudreau, B. P.: Diagenetic Models and Their Implementation: Modelling Transport and Reactions in Aquatic Sediments, Springer, Berlin and New York, 1997.

Brotas, V., Amorim-Ferreira, A., Vale, C., and Catarino, F.: Oxygen profiles in intertidal sediments of Ria Formosa (S. Portugal), Hydrobiologia, 207, 123–130, 1990.

Cook, P., Butler, E., and Eyre, B.: Carbon and nitrogen cycling on intertidal mudflats of a temperate australian estuary I. Benthic metabolism, Marine Ecol. Progr. Ser., 280, 25–38, 2004.

Ferguson, A., Eyre, B., and Gay, J.: Organic matter and benthic metabolism in euphotic sediments along shallow sub-tropical estuaries, Northern New South Wales, Australia, Aquat. Microb. Ecol., 33, 137–154, 2003a.

Ferguson, A. J. P., Eyre, B. D., and Gay, J. M.: Organic matter and benthic metabolism in euphotic sediments along shallow sub-tropical estuaries, Northern New South Wales, Australia, Aquat. Microb. Ecol., 33, 137–154, 2003b.

Frankignoulle, M., Bourge, I., and Wollast, R.: Atmospheric CO_2 fluxes in a highly polluted estuary (the scheldt), Limnol. Oceanogr., 41, 365–369, 1996.

BGD
9, 5445–5469, 2012

Frankignoulle, M., Abril, G., Borges, A., Bourge, I., Canon, C., Delille, B., Libert, E., and Théate, J.: Carbon dioxide emission from european estuaries, Science, 282, 434, 1998.
Gribsholt, B. and Kristensen, E.: Benthic metabolism and sulfur cycling along an inundation gradient in a tidal spartina anglica salt marsh, Limnol. Oceanogr., 48, 2151–2162, 2003.
Hammond, D., Giordani, P., Berelson, W., and Poletti, R.: Diagenesis of carbon and nutrients and benthic exchange in sediments of the Northern Adriatic Sea, Marine Chem., 66, 53–79, 1999.
Hargrave, B. and Phillips, G.: Annual in situ carbon dioxide and oxygen flux across a subtidal marine sediment, Estuar. Coast. Shelf Sci., 12, 725–737, 1981.
Hu, X. and Cai, W. J.: An assessment of ocean margin anaerobic processes on oceanic alkalinity budget, Global Biogeochem. Cy., 25, GB3003, 2011.
Joye, S. B., de Beer, D., Cook, P. L. M., and Perillo, G.: Biogeochemical dynamics of coastal tidal flats, in: Coastal Wetlands: an Integrated Ecosystem Approach, Elsevier, Amsterdam, 345, 2009.
Kristensen, E.: Benthic fauna and biogeochemical processes in marine sediments: microbial activities and fluxes, in: Nitrogen Cycling in Coastal Marine Environments, edited by: Blackburn, T. H. and Sorensen, J., John Wiley and Sons, Chichester, 275–299, 1988.
Lord, C. J.: A selective and precise method for pyrite determination in sedimentary materials, J. Sediment. Res., 52, 664, 1982.
Meysman, F. J. R., Middelburg, J. J., Herman, P. M. J., and Heip, C. H. R.: Reactive transport in surface sediments. II. Media: an object-oriented problem-solving environment for early diagenesis, Comput. Geosci., 29, 301–318, 2003.
Meysman, F. J. R., Boudreau, B. P., and Middelburg, J. J.: When and why does bioturbation lead to diffusive mixing?, J. Marine Res., 68, 881–920, 2010.
Middelburg, J., Klaver, G., Nieuwenhuize, J., Wielemaker, A., De Haas, W., Vlug, T., and Van der Nat, J.: Organic matter mineralization in intertidal sediments along an estuarine gradient, Marine Ecol. Progr. Ser. Oldendorf, 132, 157–168, 1996.
Migné, A., Davoult, D., Bourrand, J. J., and Boucher, G.: Benthic primary production, respiration and remineralisation: in situ measurements in the soft-bottom abra alba community of the Western English Channel (North Brittany), J. Sea Res., 53, 223–229, 2005.
Raymond, P., Bauer, J., and Cole, J.: Atmospheric CO_2 evasion, dissolved inorganic carbon production, and net heterotrophy in the York River estuary, Limnol. Oceanogr., 45, 1707–1717, 2000.

BGD
9, 5445–5469, 2012

Roy, R., Roy, L., Vogel, K., Porter-Moore, C., Pearson, T., Good, C., Millero, F., and Campbell, D.: The dissociation constants of carbonic acid in seawater at salinities 5 to 45 and temperatures 0 to 45 °C, Marine Chem., 44, 249–267, 1993.

Satienperakul, S., Cardwell, T. J., Cattrall, R. W., McKelvie, I. D., Taylor, D. M., and Kolev, S. D.: Determination of carbon dioxide in gaseous samples by gas diffusion-flow injection, Talanta, 62, 631–636, 2004.

Soetaert, K. and Meysman, F.: Reactive transport in aquatic ecosystems: rapid model prototyping in the open source software R, Environ. Model. Softw., 32, 49–60, 2012.

Soetaert, K., Petzoldt, T., and Meysman, F. J. R.: Marelac: Tools for aquatic sciences, R package version 2.1.1., 2010.

Thomas, H., Schiettecatte, L.-S., Suykens, K., Koné, Y. J. M., Shadwick, E. H., Prowe, A. E. F., Bozec, Y., de Baar, H. J. W., and Borges, A. V.: Enhanced ocean carbon storage from anaerobic alkalinity generation in coastal sediments, Biogeosciences, 6, 267–274, doi:10.5194/bg-6-267-2009, 2009.

Walling, D.: Linking land use, erosion and sediment yields in river basins, Hydrobiologia, 410, 223–240, 1999.

BGD

9, 5445–5469, 2012

Table 1. Kinetic reactions included in the reaction set.

R1:	$\{CH_2^O\}_f + O_2 \rightarrow CO_2 + H_2O$
R2:	$\{CH_2^O\}_f + 4FeOOH + 8H^+ \rightarrow 4Fe^{2+} + CO_2 + 7H_2O$
R3:	$\{CH_2^O\}_f + \frac{1}{2}SO_4^{2-} + \frac{1}{2}H^+ \rightarrow CO_2 + \frac{1}{2}HS^- + H_2O$
R4:	$\{CH_2^O\}_s + O_2 \rightarrow CO_2 + H_2O$
R5:	$\{CH_2^O\}_s + 4FeOOH + 8H^+ \rightarrow 4Fe^{2+} + CO_2 + 7H_2O$
R6:	$\{CH_2^O\}_s + \frac{1}{2}SO_4^{2-} + \frac{1}{2}H^+ \rightarrow CO_2 + \frac{1}{2}HS^- + H_2O$
R7:	$HS^- + 2O_2 \rightarrow SO_4^{2-} + H^+$
R8:	$Fe^{2+} + \frac{1}{4}O_2 + \frac{3}{2}H_2O \rightarrow FeOOH + 2H^+$
R9:	$8FeOOH + HS^- + 15H^+ \rightarrow 8Fe^{2+} + SO_4^{2-} + 12H_2O$
R10:	$Fe^{2+} + HS^- \rightarrow FeS + H^+$
R11:	$FeS + \frac{9}{4}O_2 + \frac{3}{2}H_2O \rightarrow FeOOH + SO_4^{2-} + 2H^+$
R12:	$FeS + \frac{1}{4}SO_4^{2-} + \frac{3}{4}HS^- + \frac{5}{4}H^+ \rightarrow FeS_2 + H_2O$
R13:	$FeS_2 + \frac{15}{4}O_2 + \frac{5}{2}H_2O \rightarrow FeOOH + 2SO_4^{2-} + 4H^+$

BGD
9, 5445–5469, 2012

Table 2. Kinetic rate expressions for the reactions included in the reaction set.

$$R^{f}_{min} = (1-\varphi)\, k_{fast}\, [CH_2O_f]$$

$$R^{s}_{min} = (1-\varphi)\, k_{slow}\, [CH_2O_s]$$

$$R_1 = \frac{[O_2]}{[O_2] + K_{O_2}} R^{f}_{min}$$

$$R_2 = \frac{[FeOOH]}{[FeOOH] + K_{FeOOH}} \frac{K_{O_2}}{[O_2] + K_{O_2}} R^{f}_{min}$$

$$R_3 = \frac{\left[SO_4^{2-}\right]}{\left[SO_4^{2-}\right] + K_{SO_4^{2-}}} \frac{K_{FeOOH}}{[FeOOH] + K_{FeOOH}} \frac{K_{O_2}}{[O_2] + K_{O_2}} R^{f}_{min}$$

$$R_4 = \frac{[O_2]}{[O_2] + K_{O_2}} R^{s}_{min}$$

$$R_5 = \frac{[FeOOH]}{[FeOOH] + K_{FeOOH}} \frac{K_{O_2}}{[O_2] + K_{O_2}} R^{s}_{min}$$

$$R_6 = \frac{\left[SO_4^{2-}\right]}{\left[SO_4^{2-}\right] + K_{SO_4^{2-}}} \frac{K_{FeOOH}}{[FeOOH] + K_{FeOOH}} \frac{K_{O_2}}{[O_2] + K_{O_2}} R^{s}_{min}$$

$$R_7 = \varphi k_{H_2S-Ox} [O_2] \left[HS^-\right]$$

$$R_8 = \varphi k_{Fe-Ox} \left[Fe^{2+}\right] [O_2]$$

$$R_9 = (1-\varphi)\, k_{FeOOH-H_2S} [FeOOH] \left[HS^-\right]$$

$$R_{10} = \varphi k_{FeS.form} \left[Fe^{2+}\right] \left[HS^-\right]$$

$$R_{11} = (1-\varphi)\, k_{FeS-Ox} [FeS] [O_2]$$

$$R_{12} = (1-\varphi)\, k_{FeS_2.form} [FeS] \left[HS^-\right]$$

$$R_{13} = (1-\varphi)\, k_{FeS_2-Ox} [FeS_2] [O_2]$$

BGD
9, 5445–5469, 2012

Table 3. Overview of model parameter values.

Constant	Value	Units
Porosity	0.8	–
rho.sed (density of solid sediment)	2.6	$g\,cm^{-3}$
Piston velocity	1	$cm\,h^{-1}$
K.fast (highly labile organic matter)	25	yr^{-1}
K.slow (less labile organic matter)	0.6	yr^{-1}
K_O_2 (Monod constant for O_2 consumption)	0.005	$\mu mol\,cm^{-3}$
K_FeOOH (Monod constant for FeOOH reduction)	200 · rho.sed	$\mu mol\,cm^{-3}$
K_SO_4^{2-} (Monod constant for SO_4^{2-} reduction)	1.6	$\mu mol\,cm^{-3}$
k_H_2S.Ox (Kinetic constant for H_2S oxidation)	1.6×10^7	$\mu mol^{-1}\,cm^3\,yr^{-1}$
k_Fe.Ox (Kinetic constant for Fe oxidation)	2.0×10^4	$\mu mol^{-1}\,cm^3\,yr^{-1}$
k_FeS.Ox (Kinetic constant for FeS oxidation)	160	$\mu mol^{-1}\,cm^3\,yr^{-1}$
k_FeS_2.Ox (Kinetic constant for FeS_2 oxidation)	0	$\mu mol^{-1}\,cm^3\,yr^{-1}$
k_Fe.H_2S (Kinetic constant for FeOOH/H_2S redox reaction)	2.57	$\mu mol^{-1}\,cm^3\,yr^{-1}$
k_FeS.form (Kinetic constant for FeS formation)	1×10^8	$\mu mol^{-1}\,cm^3\,yr^{-1}$
k_FeS_2.form (Kinetic constant for FeS_2 formation)	1	$\mu mol^{-1}\,cm^3\,yr^{-1}$

BGD
9, 5445–5469, 2012

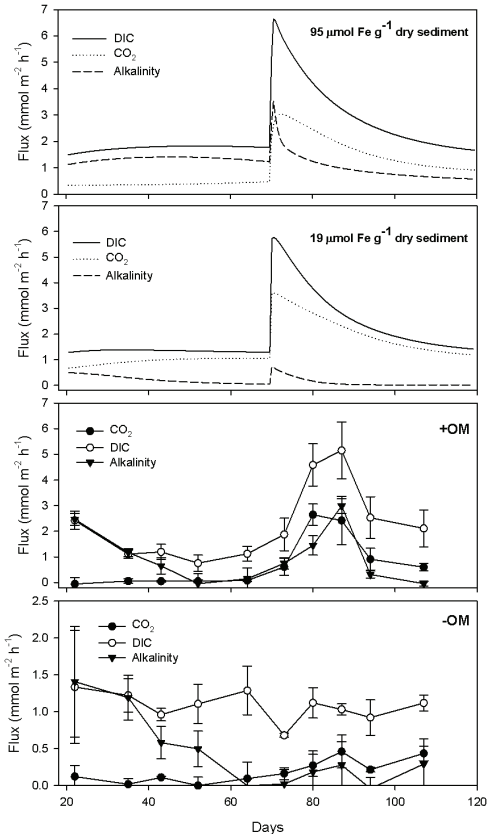

Fig. 1. Simulated mean fluxes of CO_2 during exposure (CO_2), dissolved inorganic carbon (DIC) and alkalinity during inundation in the computer simulation with 95 and 19 µmol Fe g^{-1} sediment (d/w) and laboratory core incubation fluxes with (+OM) and without (−OM) added organic matter. Error bars are standard deviations across 10 replicates.

BGD
9, 5445–5469, 2012

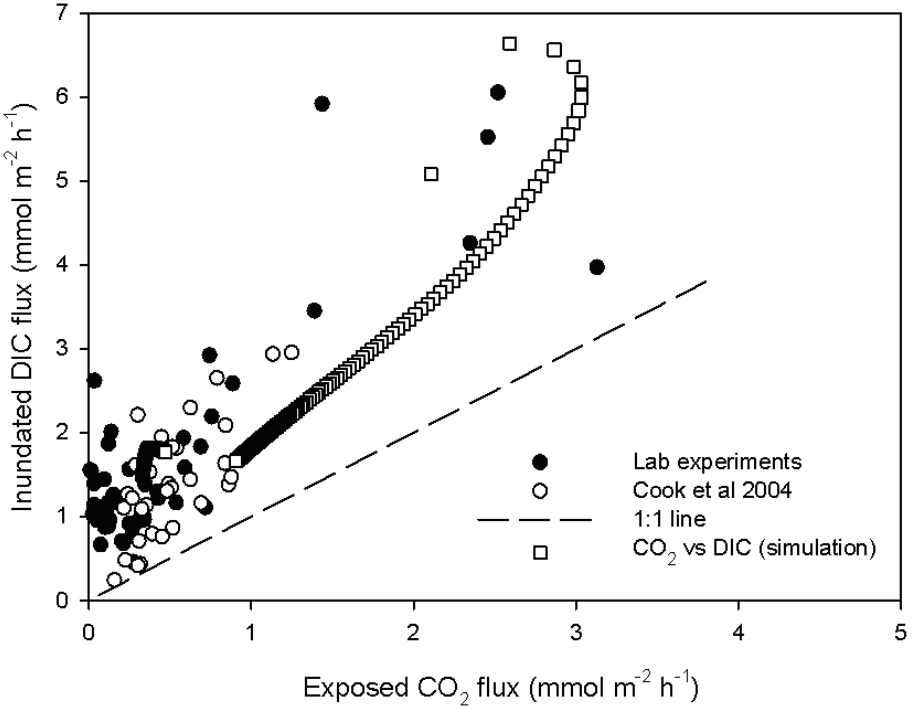

Fig. 2. Fluxes of dissolved inorganic carbon (DIC) versus exposed CO_2 fluxes for two experimental data sets, and a model simulation.

BGD
9, 5445–5469, 2012

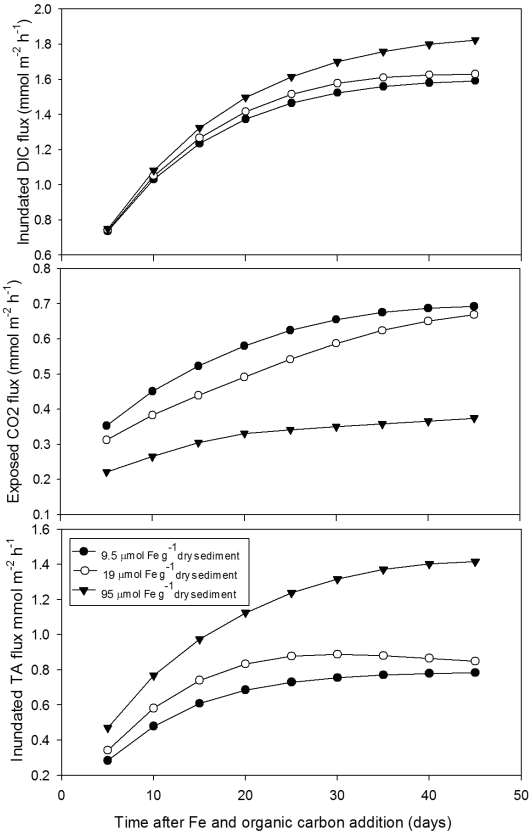

Fig. 3. Fluxes of dissolved inorganic carbon (DIC), exposed CO_2 and alkalinity fluxes for a simulation of a 50 day period with an imposed profile of 7.6, 19 and 95 μmol g^{-1} sediment (d/w) FeOOH.

BGD
9, 5445–5469, 2012

The role of alkalinity generation in controlling the fluxes of CO_2

P. A. Faber et al.

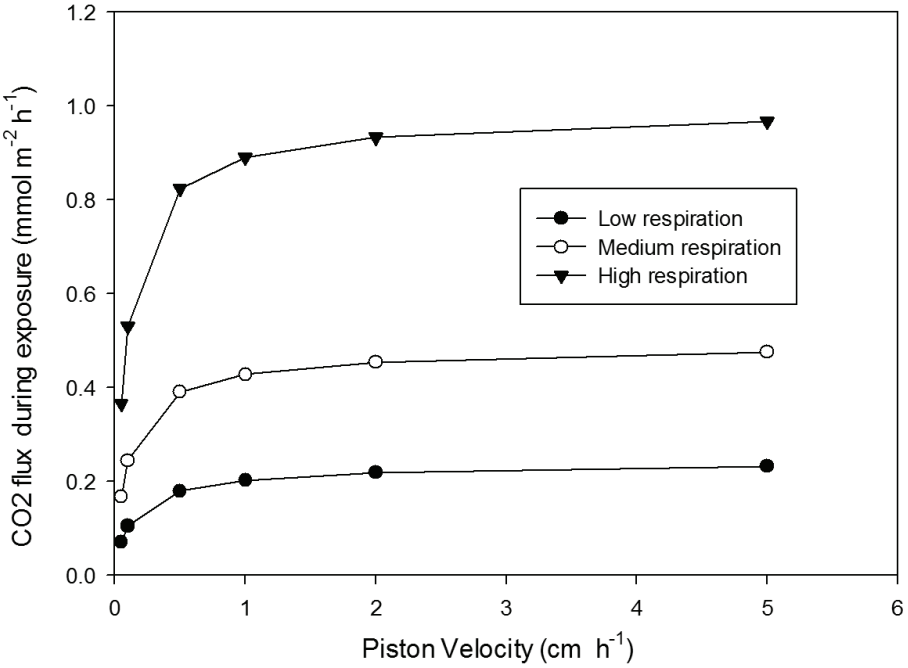

Fig. 4. Exposed flux of CO_2 with varying piston velocity and respiration rate. Low, medium and high respiration rates refer to peak DIC productions of approx. 600, 1300 and 2600 µmol m^{-2} h^{-1}, respectively.

BGD
9, 5445–5469, 2012